Report on the Effects of the Use of a Non-Zero B-angle and Interpolation in the Generation of Leakage Matrices on the Frequency-splitting Coefficients

A) Effects of the Use of a Non-Zero B-angle

In this report, we will compare the odd frequency-splitting coefficients a_1, a_3, a_5 as well as the sum $a_1+a_3+a_5$ that were computed from the tables of fitted mode parameters HMI.100430to0710b-6.354.v0 and HMI.100430to0710.v7, respectively. Both tables were generated with the MPTS method and are based on the same 72-day observing run of the HMI which began on April 30 of 2010. For the generation of the "v7" table, the reference set of leaks corresponding to a B-angle of zero were used, while for the generation of the "v0" table leaks corresponding to a B-angle of -6.354 degrees were used. The leaks for the B-angle of -6.354 degrees were kindly generated by Dr. Larson. For the remainder of this report, we will refer to this case of using different B-angles in the generation of the two sets of leakage matrices as the "Bang" case.

In Table 1 we have listed the averages and standard deviations of the raw and normalized differences of the odd frequency-splitting coefficients a_1, a_3, a_5, respectively, and the sum $a_1+a_3+a_5$. In addition to computing the averages and standard deviations of both the raw and normalized coefficient differences, we also employed Student's t-Test to determine whether those two averages were significantly different from zero. The absolute magnitude of the t-value and the probability that the corresponding sample difference occurred by chance are listed in the columns labeled $|t|$ and p, respectively. All eight of these probabilities were so close to zero that we can reject the null hypothesis that each of these averages was equal to zero. All eight of these differences were computed in the sense HMI.100430to0710.v7 minus HMI.100430to0710b-6.354.v0.

difference mode parameter	$n_{\rm d}$	raw				normalized			
		ave	std	$\lvert t\rvert$	p	ave	std	$\lvert t\rvert$	p
a_1	7307	-0.1055	1.7036	5.294	≈ 0	-0.5534	0.5621	84.154	≈ 0
a_3	7283	$+0.1579$	1.7099	7.883	≈ 0	$+0.7726$	0.9077	72.643	≈ 0
a_5	7001	-0.1866	0.6383	24.455	≈ 0	-0.8166	0.8041	84.982	≈ 0
$a_1+a_3+a_5$	7001	-0.1348	2.4012	4.697	≈ 0	-0.2261	0.4549	41.585	≈ 0

Table 1: Averages and standard deviations of both the raw and normalized differences of the odd frequency-splitting coefficients a_1, a_3, a_5, and the sum $a_1+a_3+a_5$, as obtained from the tables of fitted mode parameters HMI.100430to0710b-6.354.v0 and HMI.100430to0710.v7, respectively. All types of differences were computed in the sense HMI.100430to0710.v7 minus HMI.100430to0710b-6.354.v0. The normalizaton was carried out by dividing the raw differences by the formal error of each difference. Using Student's t-Test, each mean raw and each mean normalized frequency difference was tested for a significant deviation from zero. The absolute magnitude of the t-value and the probability that the sample difference occurred by chance are listed in the columns labeled $|t|$ and p, respectively. The reason we are showing $|t|$ is because we are employing a one-sided hypothesis test (i.e., H_0 : ave $= 0$). Since we are using a one-sided test, it is irrelevant whether ave < 0 or ave > 0. In the column labeled $n_{\rm d}$ the number of data points are given. The raw differences of the frequency-splitting coefficients are measured in nHz.

In Figure 1 we show in magenta the odd HMI.100430to0710.v7 frequency-splitting coefficients

a_1, a_3, a_5, as well as their sum $a_1 + a_3 + a_5$, for the $n = 0$ ridge, as function of the spherical harmonic degree. In black are shown the corresponding HMI.100430to0710b-6.354.v0 frequency-splitting coefficients. Inspection of Figure 1 shows that the a_1, a_5, and $a_1 + a_3 + a_5$ splitting coefficients that were computed using the non-zero B-angle (the black curves) were higher than the corresponding coefficients that were computed using the reference leakage matrices (the magenta curves), while the non-zero B-angle a_3 coefficients were smaller than the corresponding reference coefficients. These shifts in the four sets of coefficients are consistent with the signs of the average raw differences that are contained in Table 1. This is the case because the sense of all of the subtractions in this section was HMI.100430to0710.v7 minus HMI.100430to0710b-6.354.v0.

For comparison we also shown in red the 2010 SKh(67d) frequency-splitting coefficients obtained with the fitting methodology of Korzennik, and in green the 2010 JS(67d) frequency-splitting coefficients obtained with the mean-multiplet technique of Schou. As we explained in great detail in our November 2021 Progress Report, a copy of which can be provided upon request, the jumps around $l \approx 400$ in the black and magenta curves which cannot be adequately represented by a rotational inversion are not caused by any artefacts in the seed coefficients that we employed in our fitting runs using the MPTS method. The fact that the jumps that are seen in the a_1, a_3, and a_5 coefficients are barely visible in their sum suggests that the flow gradients that are the cause of these jumps are a function of latitude and are very weak at the solar equator.

In Figure 2 we show the raw, and in Figure 3 the normalized differences in the odd frequency-splitting coefficients a_1, a_3, a_5, as well as in their sum $a_1 + a_3 + a_5$ as a function of the spherical harmonic degree for the ridges $n = 0$ (black diamonds) and $n = 1$ (red triangles). Both Figures demonstrate that the differences in the coefficients for both the $n = 0$ and $n = 1$ ridges are small but systematically different from zero. Only a few outliers exceed the $3\,\sigma$ level. The left-hand panels in Figure 2 show that the differences in the a_1 and a_5 coefficients were mainly negative for $l > 350$ for the $n = 0$ ridge (the black curves) and for $l > 250$ for the $n = 1$ ridge (the red curves). The signs of these higher-degree differences agree with the signs of the corresponding raw averages in Table 1. The upper-right panel of Figure 2 shows that the signs of the a_3 differences were mainly positive for $l > 350$ for the $n = 0$ ridge and for $l > 250$ for the $n = 1$ ridge. This sign is also consistent with the sign of the corresponding raw average in Table 1. The lower-right panel of Figure 2 shows that the predominant sign of the differences in the $a_1 + a_3 + a_5$ coefficients was also negative, in agreement with the sign of the corresponding raw average in Table 1.

In Figure 3 we show the normalized coefficient differences for the Bang comparison. All four panels of Figure 3 show the same predominant signs for the differences as were shown in the corresponding panels of Figure 2. The major differences between Figures 2 and 3 are the facts that the normalization process has introduced some curvature into the a_1, a_3, and a_5 coefficient differences for the $n = 0$ ridge (the black curves) and it has reversed the curvature of the $n = 1$ ridge (the red curves). In contrast, the normalization process has not altered the differences in $a_1 + a_3 + a_5$ for either ridge.

We recently extended our analyses to include the odd-order coefficients for all 31 ridges rather than just the $n = 0$ and $n = 1$ ridges that we have discussed above. We examined the differences in the frequency-splitting coefficients as a function of both degree and frequency. However, it was readily evident that the differences in the sets of coefficients were much more single-valued when displayed as a function of degree rather than frequency. Hence, we will only show plots as functions of degree here.

In Figure 4 we show the raw differences in the odd frequency-splitting coefficients a_1, a_3, a_5, as well as in their sum $a_1 + a_3 + a_5$ for all 31 ridges as a function of the spherical harmonic degree for the Bang comparison. All four panels of Figure 4 look very similar to the corresponding panels of Figure 2. The $n = 0$ and $n = 1$ ridges are distinct at the high-degree side of the two upper panels

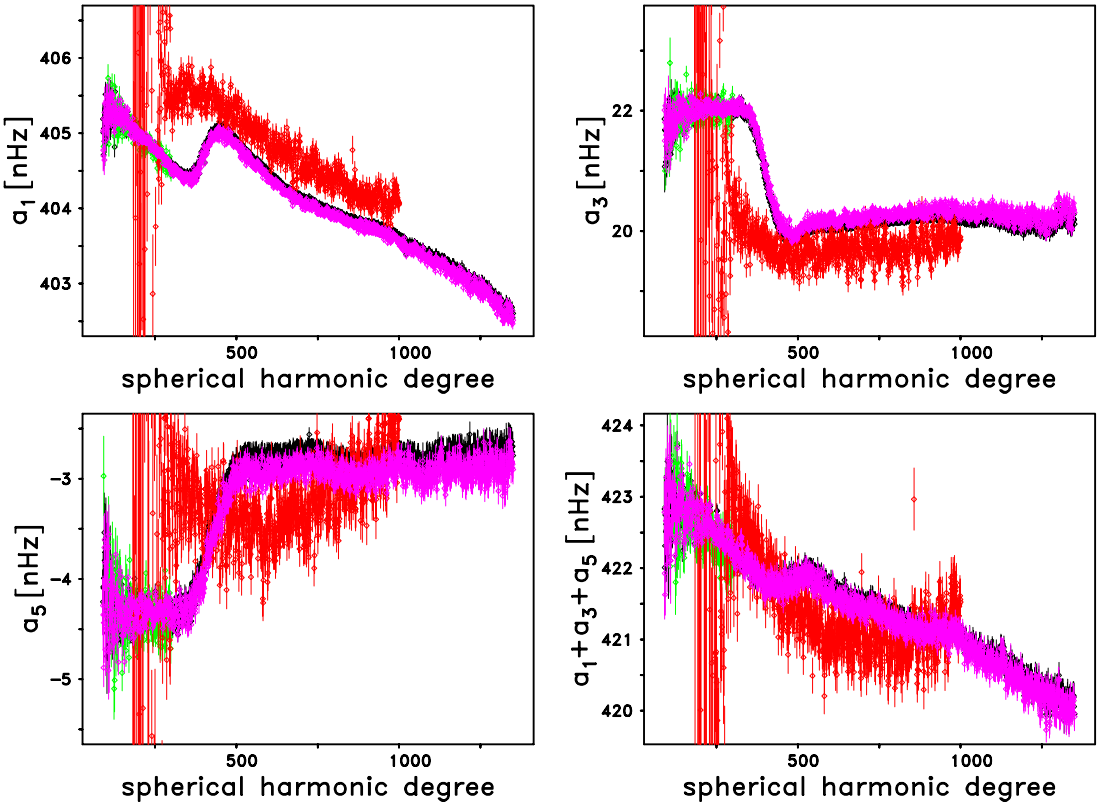

Figure 1: Dependency of the frequency-splitting coefficients a_1 (upper-left), a_3 (upper-right), a_5 (lower-left), and their sum $a_1 + a_3 + a_5$ (lower-right) for the $n = 0$ ridge on the spherical harmonic degree. In black are shown the frequency-splitting coefficients HMI.100430to0710b-6.354.v0, while in magenta are shown the frequency-splitting coefficients HMI.100430to0710.v7. For comparison are shown in red the 2010 SKh(67d) frequency-splitting coefficients obtained with the fitting methodology of Korzennik, and in green the 2010 JS(67d) frequency-splitting coefficients obtained with the mean-multiplet technique of Schou.

and the lower-left panel in Figure 4. The high-degree ends of the $n = 2$, 3, and 4 ridges are also evident in the same panels, but the coefficient differences for all of the higher order ridges blend together for $l < 500$.

While we were preparing this report, Dr. Jesper Schou sent us a reference to Schou *et al.* (2002) in which he and his co-authors studied the effects upon rotational inversions of the use of 12 different sets of splitting coefficients that they computed using both the GONG and MDI observations at three different levels of solar activity. Specifically, these authors generated four different tables at each of the different levels of activity. One of these four splitting coefficient tables came from the application of the GONG data processing pipeline, which they referred to as the "AZ" pipeline, to a time series of GONG observations. The second frequency table came from the application of the AZ pipeline to a simultaneous set of MDI observations. The third table came from the application of the Stanford pipeline, which these authors referred to as the "CA" pipeline to the set of MDI observations, while the fourth table came from the application of the CA pipeline to the set of GONG observations. Since these authors included their Figure 4 in which they showed all four sets of splitting coefficients for their low activity observing run as functions of frequency and they also presented comparisons of the results of rotational inversions using these four tables, we compared

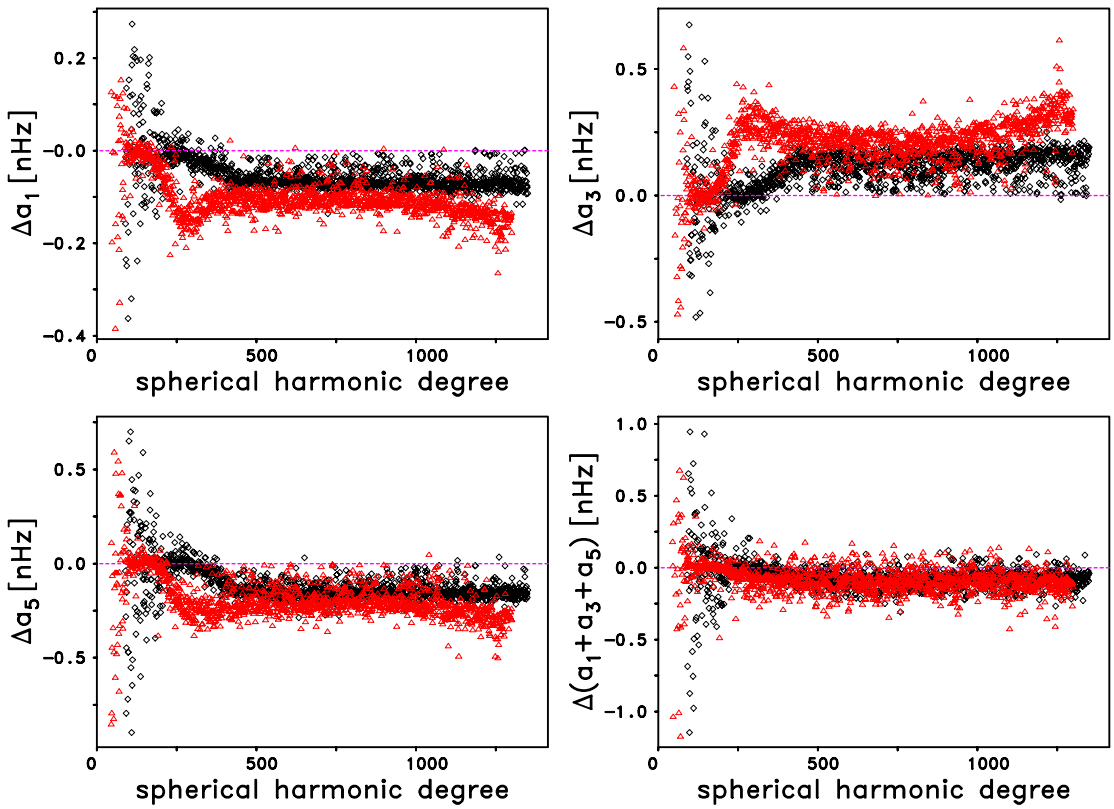

Figure 2: (Upper-left panel) Raw differences $\Delta a_1 = a_{1_{\rm HMI.100430to0710.v7}} - a_{1_{\rm HMI.100430to0710b-6.354.v0}}$ of the frequency-splitting coefficients a_1 as functions of the spherical harmonic degree for the ridges $n = 0$ (black diamonds) and $n = 1$ (red triangles). The dashed magenta line is for a difference of zero. (Upper-right panel) Same as upper-left panel, but for the frequency-splitting coefficients a_3. (Bottom-left panel) Same as upper-left panel, but for the frequency-splitting coefficients a_5. (Bottom-right panel) Same as bottom-left panel, but for the sum of the odd frequency-splitting coefficients $a_1 + a_3 + a5$.

our Bang coefficient differences with the differences presented in their Figure 4.

This comparison showed that the largest differences in the a_1 coefficient that were shown in Figure 4 of Schou *et al.* (2002) were about five times larger than most of the differences shown in the upper-left hand panel of our Figure 4, while the largest differences in their a_3 coefficients were about ten times larger than the majority of the differences shown in the upper-right hand panel of our Figure 4, and the largest differences in their a_5 coefficients were about ten times larger than the majority of the differences that are shown in the lower-left hand panel of our Figure 4.

Based upon the differences in the resulting rotational inversions that Schou *et al.* (2002) presented in their Figure 6, we would expect to see some small but systematic differences in the rotational inversions that would result from our two tables of MPTS splitting coefficients.

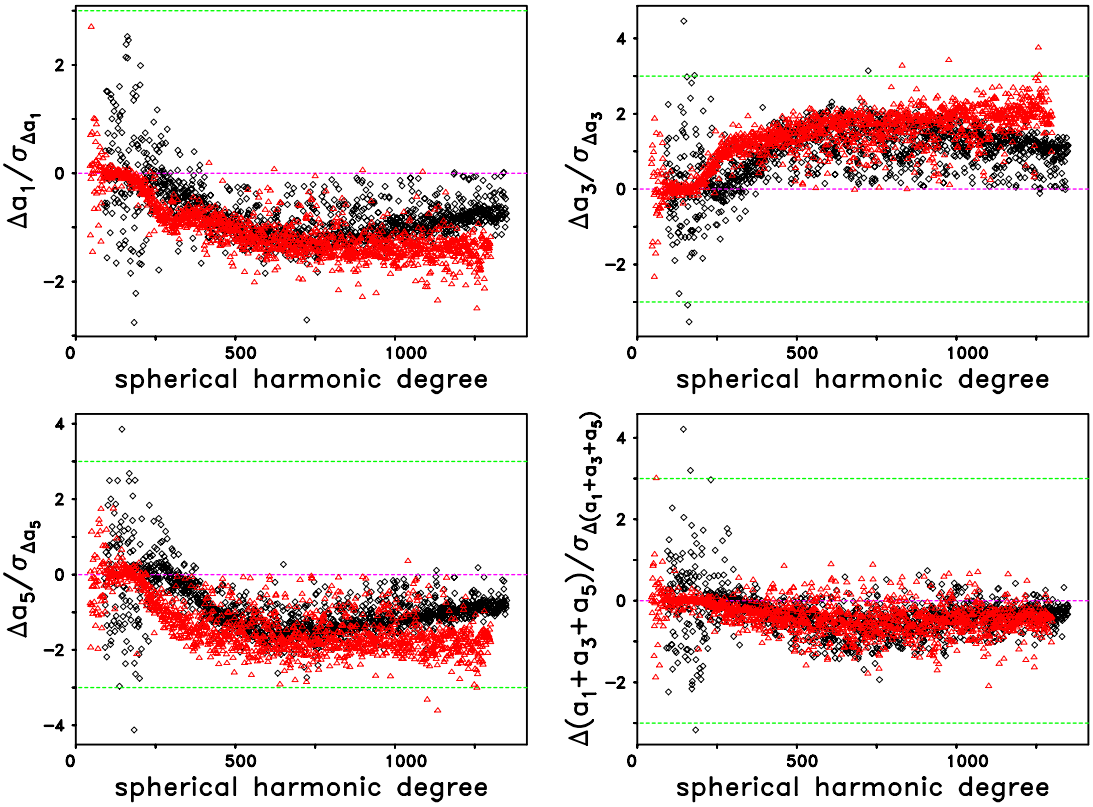

Figure 3: Same as Figure 2, but for the normalized differences $\Delta a_1 = a_{1_{\mathrm{HMI.100430to0710.v7}}} - a_{1_{\mathrm{HMI.100430to0710b-6.354.v0}}}$ The normalization was carried out by dividing the raw differences, Δa_1, as shown in the upper left-hand panel of Figure 2, by the formal error, $\sigma_{\Delta a_1}$, of each difference.

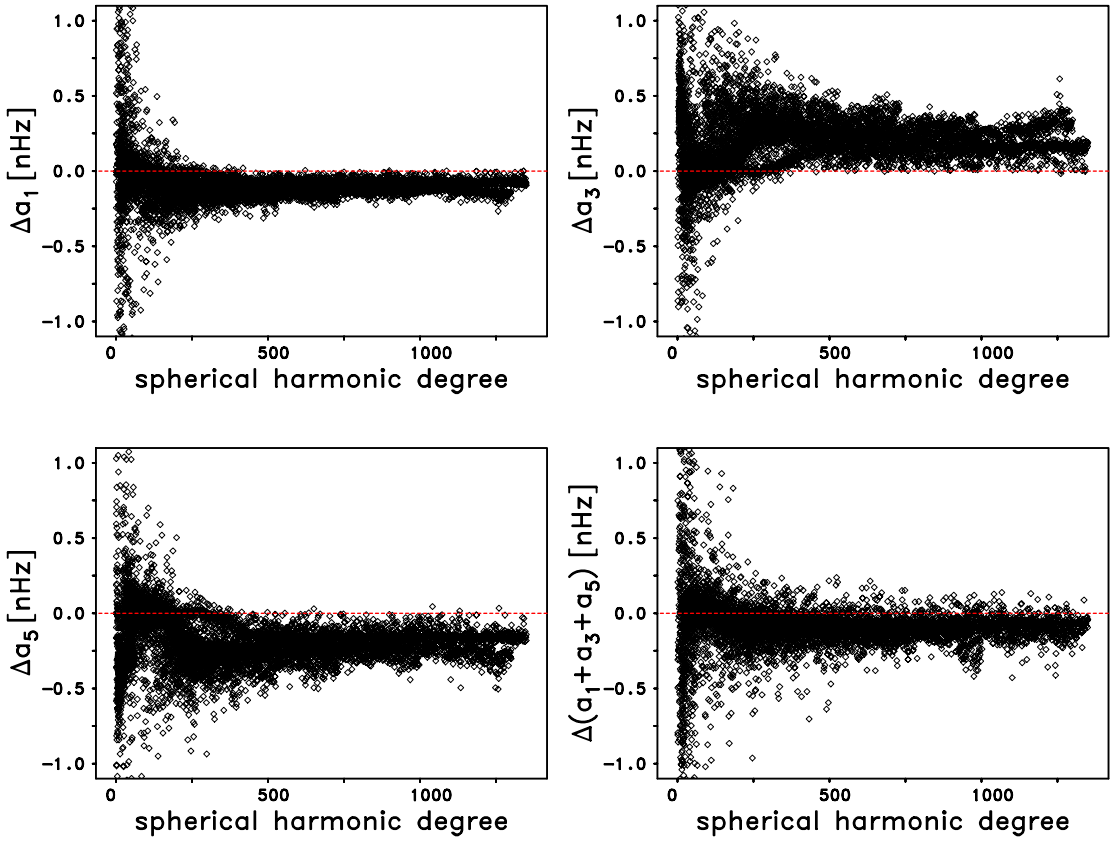

Figure 4: (Upper-left panel) Raw differences $\Delta a_1 = a_{1_{\mathrm{HMI.100430to0710.v7}}} - a_{1_{\mathrm{HMI.100430to0710b-6.354.v0}}}$ of the frequency-splitting coefficients a_1 as functions of the spherical harmonic degree for the ridges $n = 0$ through $n = 30$. The dashed red line is for a difference of zero. (Upper-right panel) Same as upper-left panel, but for the frequency-splitting coefficients a_3. (Bottom-left panel) Same as upper-left panel, but for the frequency-splitting coefficients a_5. (Bottom-right panel) Same as bottom-left panel, but for the sum of the odd frequency-splitting coefficients $a_1 + a_3 + a5$.

In Figure 5, we show the normalized differences in the same splitting coefficients. The two upper-row panels and the lower-left panel show systematic differences in all three of the coefficients which are as large as between 2 and $3\,\sigma$ in magnitude. The lower-right panel shows systematic, but smaller differences in the sum of the three coefficients. We present some statistics related to the raw splitting coefficient differences in Table 2. In the first two rows of this table, we show that between 25 and 45 percent of the differences exceeded $1\,\sigma$ in size, while nearly five percent of the a_3 and a_5 coefficient differences exceeded $2\,\sigma$. The last column of Table 2 shows that negligible numbers of these coefficient differences exceed $3\,\sigma$. The last row of this table shows that nearly 96 percent of differences in the sums of all three coefficients were less than $1\,\sigma$ in size. This point means that the systematic differences in the three coefficients will mainly result in differences in rotational inversions away from the solar equatorial plane.

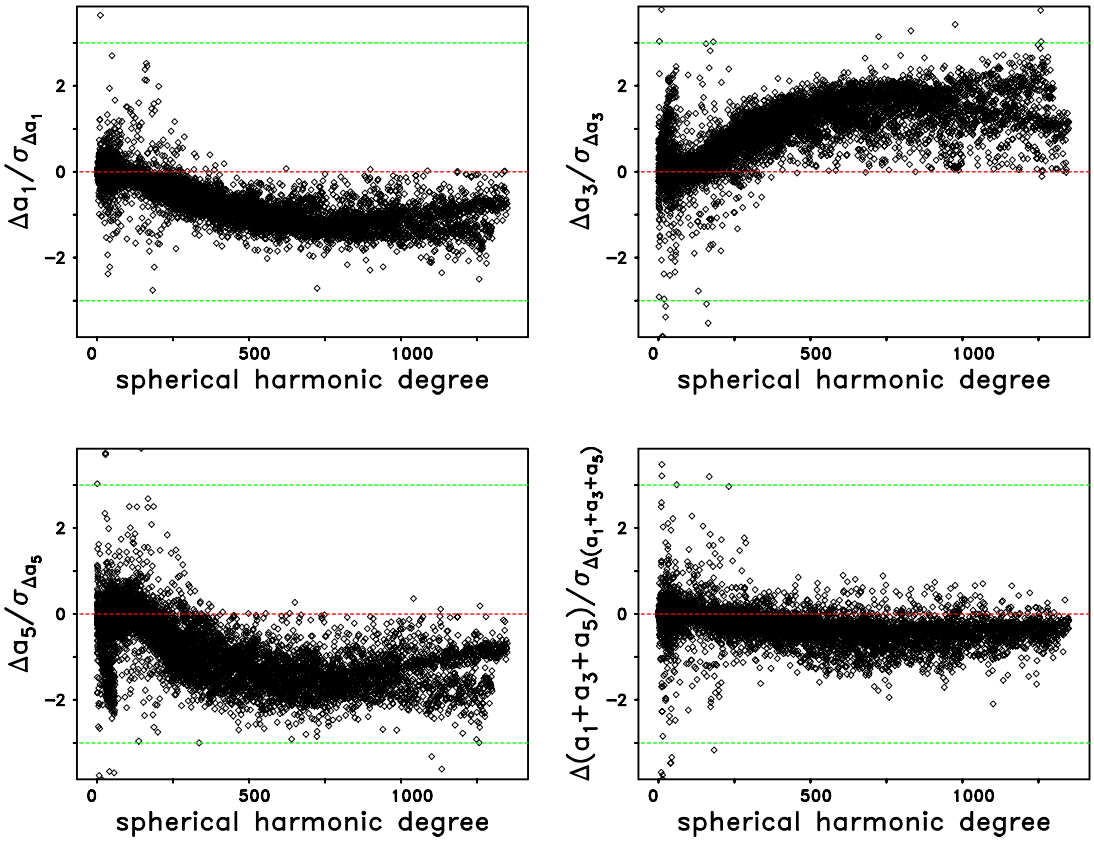

Figure 5: Same as Figure 4, but for the normalized differences $(a_{1_{\mathrm{HMI.100430to0710.v7}}} - a_{1_{\mathrm{HMI.100430to0710b-6.354.v0}}})/\sigma_{\Delta a_1}$ The normalization was carried out by dividing the raw differences, Δa_1, as shown in the upper left-hand panel of Figure 4, by the formal error, $\sigma_{\Delta a_1}$, of each difference. The dashed green lines show the $\pm 3\,\sigma$ levels.

difference	#	$\% > 1\,\sigma$	$\% > 2\,\sigma$	$\% > 3\,\sigma$
a_1	7307	25.43	0.37	0.03
a_3	7283	42.22	4.90	0.59
a_5	7001	44.34	4.80	0.34
$a_1 + a_3 + a_5$	7001	4.59	0.59	0.30

Table 2: Statistics of the differences in the odd frequency-splitting coefficients as well as in their sum. In the 2nd column the number of commom cases is listed. The remaining columns give the percentages of cases for which the differences exceed the $1\,\sigma$, $2\,\sigma$, and $3\,\sigma$ level, respectively.

In Figure 6 we show the binned raw differences in the splitting coefficients as functions of degree. The error bars are the standard errors of the means in each of the 100-degree wide bins. All four panels of this figure show that in most of the cases the average differences were many standard errors away from zero. All four of these panels also show that the binned raw differences were relatively constant for degrees greater than 200. In Figure 7 we show the binned normalized coefficient differences as functions of degree. The upper-right and lower-left panels show that the normalized coefficient differences were as large as $1.5\,\sigma$. Furthermore, all four panels show that, with the exception of the two lowest bins, all of the other normalized differences are multiple standard errors away from zero. In contrast to the results shown in Figure 6, the four panels of this figure show that the binned normalized coefficient differences varied strongly with increasing degree up to $l = 800$ before leveling off until $l = 1300$ and dropping slightly for the $n = 0$ ridge for degrees between 1301 and 1350.

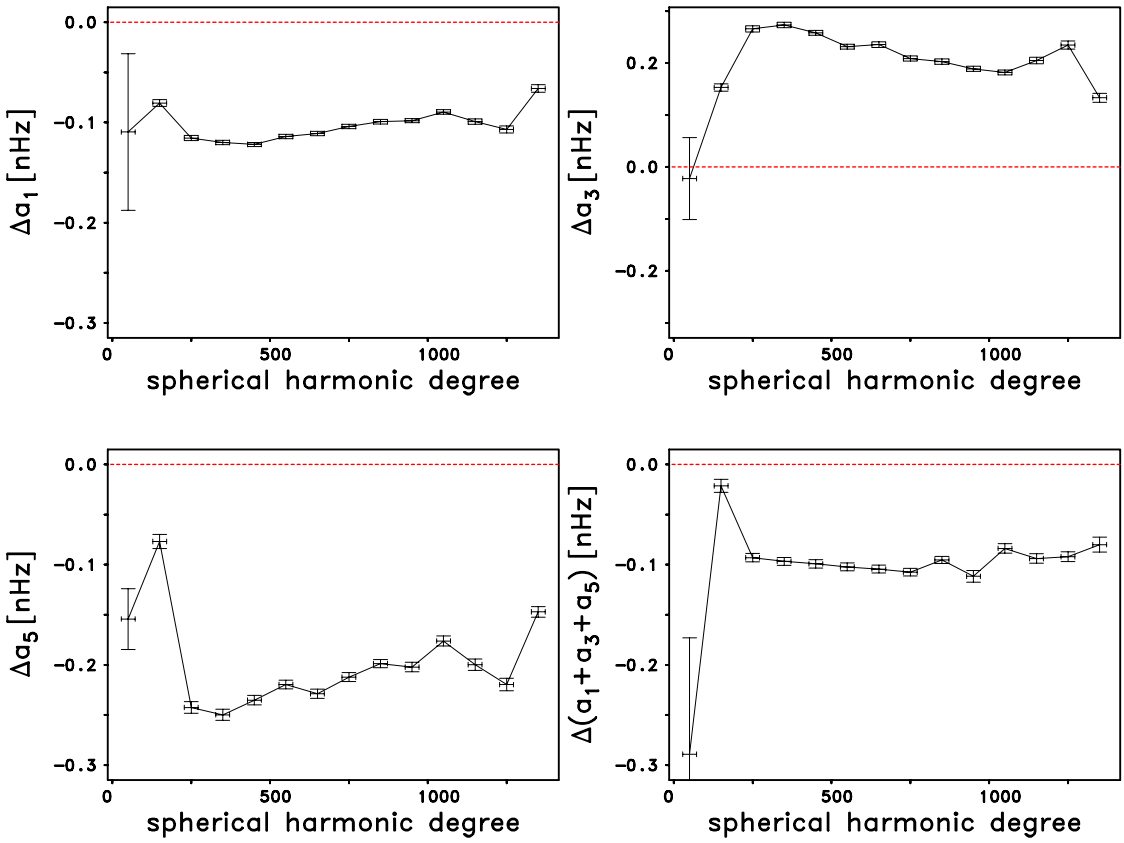

Figure 6: (Upper-left panel) Binned raw differences $\Delta a_1 = a_{1_{\mathrm{HMI.100430to0710.v7}}} - a_{1_{\mathrm{HMI.100430to0710b-6.354.v0}}}$ of the frequency-splitting coefficients a_1 as functions of the spherical harmonic degree using 100-degree wide bins for the ridges $n = 0$ through $n = 30$. The dashed red line is for a difference of zero. (Upper-right panel) Same as upper-left panel, but for the frequency-splitting coefficients a_3. (Bottom-left panel) Same as upper-left panel, but for the frequency-splitting coefficients a_5. (Bottom-right panel) Same as bottom-left panel, but for the sum of the odd frequency-splitting coefficients $a_1 + a_3 + a5$.

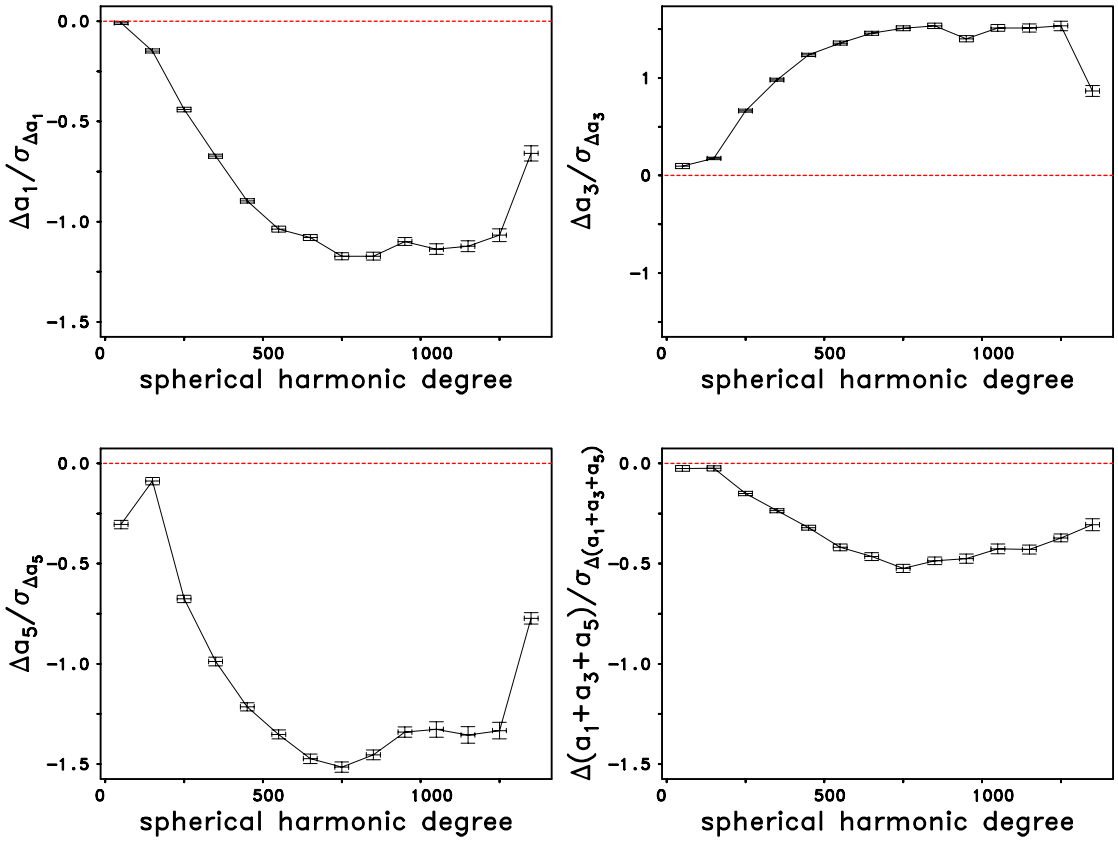

Figure 7: Same as Figure 6, but for the normalized differences $(a_{1_{\mathrm{HMI.100430to0710.v7}}} - a_{1_{\mathrm{HMI.100430to0710b-6.354.v0}}})/\sigma_{\Delta a_1}$ The normalization was carried out by dividing the raw differences, Δa_1, as shown in the upper left-hand panel of Figure 4, by the formal error, $\sigma_{\Delta a_1}$, of each difference.

B) Effects of Interpolation in the Generation of the Leakage Matrices on the Frequency-splitting Coefficients

In this section, we compare the the odd frequency-splitting coefficients a_1, a_3, a_5 as well as the sum $a_1 + a_3 + a_5$ for the $n = 0$ ridge that came from the same HMI.100430to0710.v7 table that was employed in Section A) above with the corresponding parameters that came from a third table of mode parameters that we named HMI.100430to0710.i.v0, respectively. While for the generation of the "v7" table the complete set of reference leaks which corresponded to the B-angle of zero were used, for the generation of the "i.v0" table an interpolated version of the same reference set of leaks was used instead. The interpolated table of the reference set of leaks was kindly generated by Dr. Tim Larson. For the remainder of this report, we will refer the case of interpolated leakage matrices as the "iplkm" case.

In Table 3 we list the averages and standard deviations of both the raw and normalized differences of the odd frequency-splitting coefficients a_1, a_3, a_5, respectively, and the sum $a_1 + a_3 + a_5$. Each difference was computed in the sense HMI.100430to0710.i.v0 minus HMI.100430to0710.v7. Keeping in mind the fact that this sense of subtractions is opposite to that employed in Section A), we see that if we flip the signs of all eight of the averages that are shown in Table 3, seven of them will agree with the corresponding signs of the averages in Table 1. Only the flipped sign of the $a_1 + a_3 + a_5$ differences would be different from the corresponding sign in Table 1, and this average happens to be the smallest of all eight of the raw averages.

difference		raw				normalized			
mode parameter	$n_{\rm d}$	ave	std	$\lvert t\rvert$	p	ave	std	$\lvert t\rvert$	p
a_1	7307	+0.0179	1.4623	1.045	0.296	+0.3137	0.6662	40.252	≈ 0
a_3	7282	−0.0569	1.6796	2.892	0.004	−0.3577	0.8951	34.103	≈ 0
a_5	7013	+0.0354	0.5851	5.069	≈ 0	+0.2758	0.6682	34.568	≈ 0
$a_1 + a_3 + a_5$	7013	−0.0055	2.1863	0.212	0.832	+0.0808	0.3837	17.628	≈ 0

Table 3: Averages and standard deviations of both the raw and normalized differences of the odd frequency-splitting coefficients a_1, a_3, a_5, and the sum $a_1 + a_3 + a_5$, as obtained from the tables of fitted mode parameters HMI.100430to0710.i.v0 and HMI.100430to0710.v7, respectively. All types of differences were computed in the sense HMI.100430to0710.i.v0 minus HMI.100430to0710.v7. The normalizaton was carried out by dividing the raw differences by the formal error of each difference. Using Student's t-Test, each mean raw and each mean normalized frequency difference was tested for a significant deviation from zero. The absolute magnitude of the t-value and the probability that the sample difference occurred by chance are listed in the columns labeled $|t|$ and p, respectively. The reason we are showing $|t|$ is because we are employing a one-sided hypothesis test (i.e., H_0 : ave $= 0$). Since we are using a one-sided test, it is irrelevant whether ave < 0 or ave > 0. In the column labeled $n_{\rm d}$ the number of data points are given. The raw differences of the frequency-splitting coefficients are measured in nHz.

The absolute magnitude of the t-value and the probability that the corresponding sample difference occurred by chance are listed in the columns labeled $|t|$ and p, respectively, in Table 3. In contrast to the Bang case, for which all eight of the probabilities were very close to zero, the probabilities for the raw a_1 and the raw $a_1 + a_3 + a_5$ iplkm coefficient differences are both so large that we can accept the null hypothesis for those two groups of raw differences. On the other hand, using the 1 % significance level, we can reject the null hypothesis for the raw iplkm a_3 and a_5 differences and for all four of the normalized iplkm differences.

In Figure 8 we show in magenta the odd HMI.100430to0710.v7 frequency-splitting coefficients a_1, a_3, a_5, as well as their sum $a_1 + a_3 + a_5$, for the $n = 0$ ridge, as function of the spherical harmonic degree. In black are shown the corresponding HMI.100430to0710.i.v0 frequency-splitting coefficients. For comparison are also shown in red the 2010 SKh(67d) frequency-splitting coefficients obtained with the fitting methodology of Korzennik, and in green the 2010 JS(67d) frequency-splitting coefficients obtained with the mean-multiplet technique of Schou.

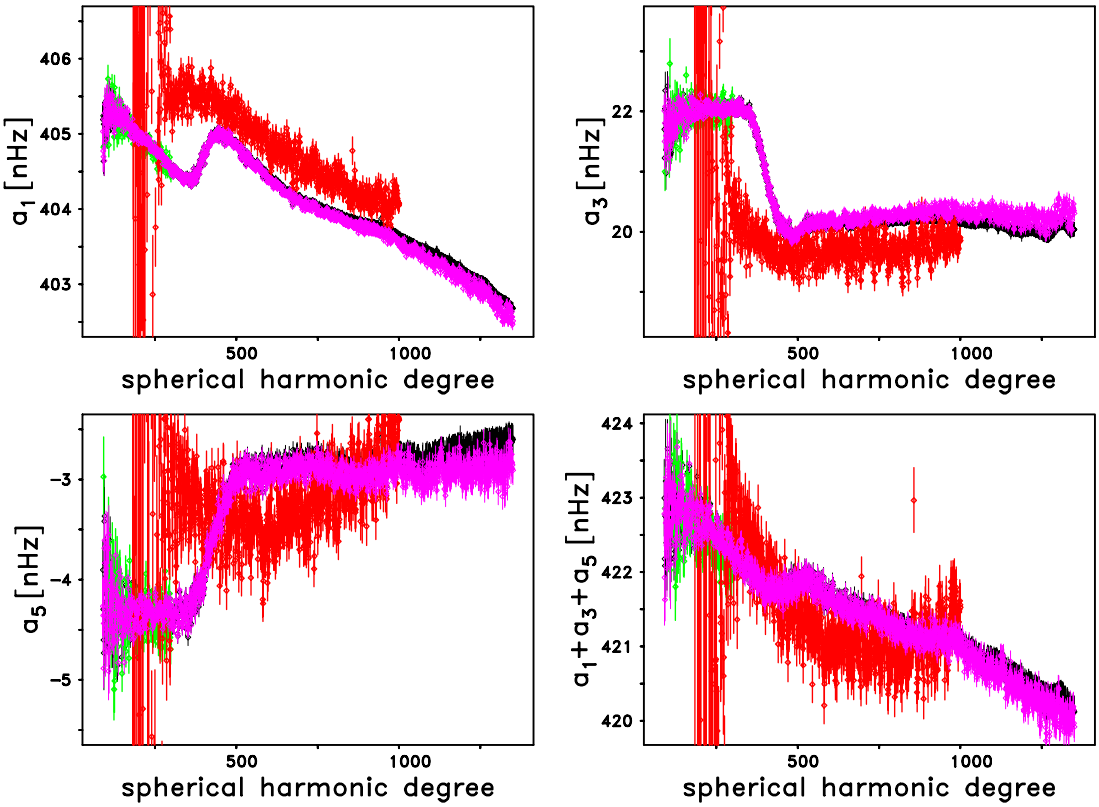

Figure 8: Dependency of the frequency-splitting coefficients a_1 (upper-left), a_3 (upper-right), a_5 (lower-left), and their sum $a_1+a_3+a_5$ (lower-right) for the $n = 0$ ridge on the spherical harmonic degree. In black are shown the frequency-splitting coefficients HMI.100430to0710.i.v0, while in magenta are shown the frequency-splitting coefficients HMI.100430to0710.v7. For comparison are shown in red the 2010 SKh(67d) frequency-splitting coefficients obtained with the fitting methodology of Korzennik, and in green the 2010 JS(67d) frequency-splitting coefficients obtained with the mean-multiplet technique of Schou.

In Figure 9 we show the raw, and in Figure 10 the normalized differences in the odd frequency-splitting coefficients a_1, a_3, a_5, as well as in their sum $a_1 + a_3 + a_5$ as a function of the spherical harmonic degree for the ridges $n = 0$ (black diamonds) and $n = 1$ (red triangles). Both Figures demonstrate that the use of interpolateded leakage matrices did result in systematic differences in those coefficients. For the $n = 1$ ridge, the normalized differences exceed the $3\,\sigma$ level for the highest degrees.

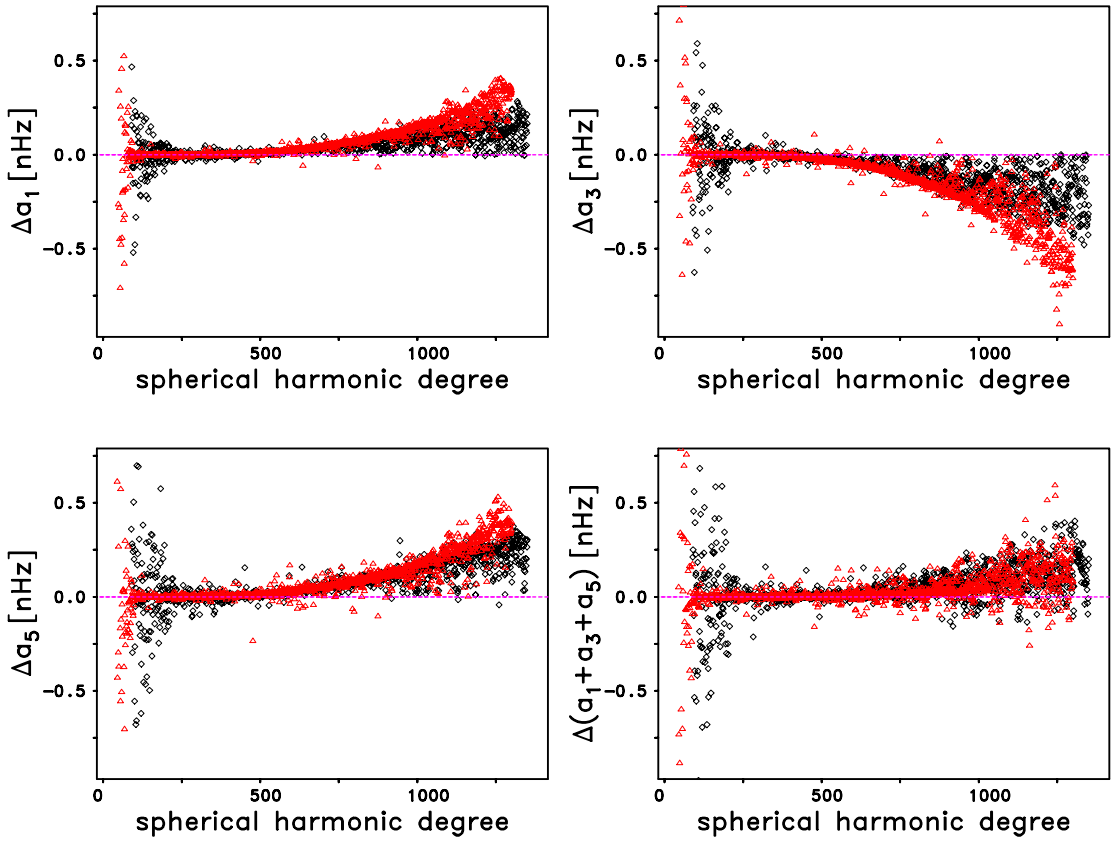

Figure 9: (Upper-left panel) Differences $\Delta a_1 = a_{1_{\rm HMI.100430to0710.i.v0}} - a_{1_{\rm HMI.100430to0710.v7}}$ of the frequency-splitting coefficients a_1 as functions of the spherical harmonic degree for the ridges $n = 0$ (black diamonds) and $n = 1$ (red triangles). The dashed magenta line is for a difference of zero. (Upper-right panel) Same as upper-left panel, but for the frequency-splitting coefficients a_3. (Bottom-left panel) Same as upper-left panel, but for the frequency-splitting coefficients a_5. (Bottom-right panel) Same as bottom-left panel, but for the sum of the odd frequency-splitting coefficients $a_1 + a_3 + a5$.

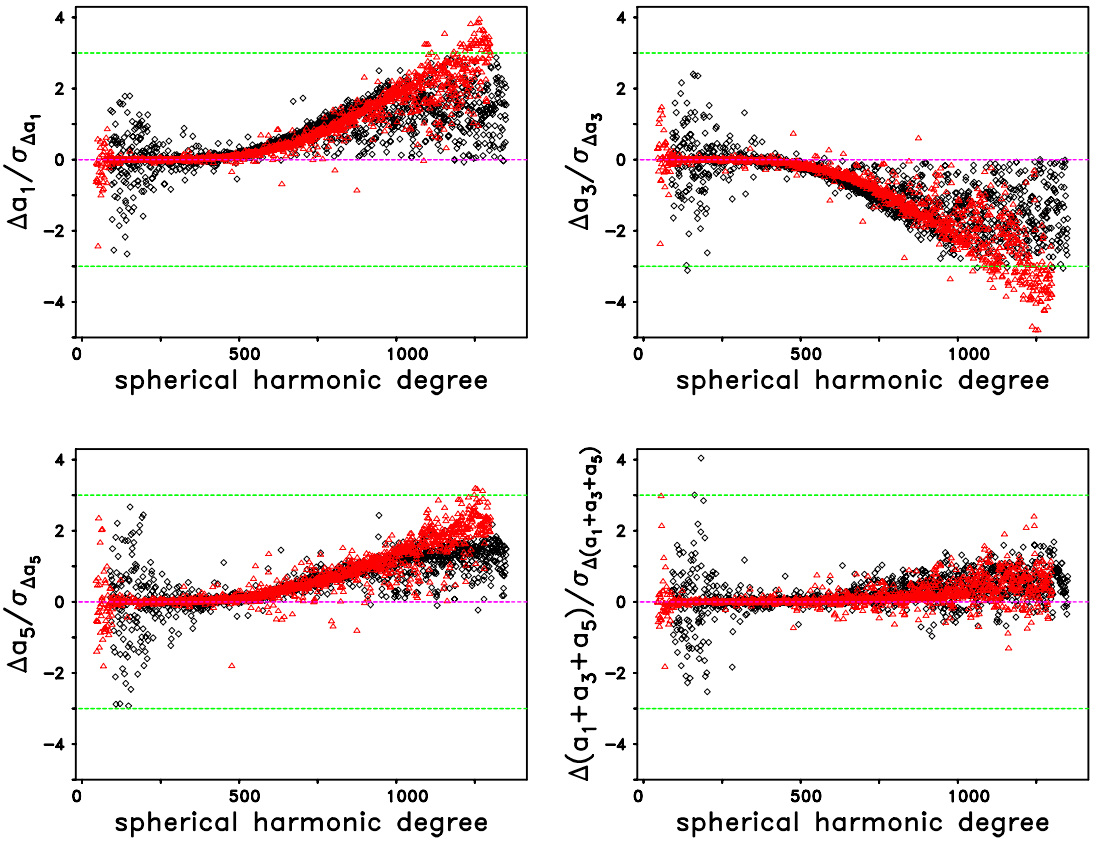

Figure 10: (Upper-left panel) Normalized differences $\Delta a_1 = a_{1_{\rm HMI.100430to0710.i.v0}} - a_{1_{\rm HMI.100430to0710.v7}}$ of the frequency-splitting coefficients a_1 as functions of the spherical harmonic degree for the ridges $n = 0$ (black diamonds) and $n = 1$ (red triangles). The normalization was carried out by dividing the raw differences, Δa_1, as shown in the upper left-hand panel of Figure 9, by the formal error, $\sigma_{\Delta a_1}$, of each difference. The dashed green line shows the $+3\,\sigma$ value. The dashed magenta line is for a difference of zero. (Upper-right panel) Same as upper-left panel, but for the frequency-splitting coefficients a_3. (Bottom-left panel) Same as upper-left panel, but for the frequency-splitting coefficients a_5. (Bottom-right panel) Same as bottom-left panel, but for the sum of the odd frequency-splitting coefficients $a_1 + a_3 + a5$.

We show the raw differences in the three splitting coefficients and in their sum that resulted from our iplkm comparison in Figure 11. All four of these panels show that the differences scatter randomly for degrees below about 75 before dropping in size up to a degree of 500. For the degrees above $l = 500$, all four panels show a smooth upper limit of the differences that increases with increasing degree, while spread in the sizes of the differences increasing with increasing degree as well. Excluding the large, random differences shown in both Figures 2 and 11 for degrees below 75, the largest differences shown in Figure 11 are slightly larger than the largest differences shown in Figure 4.

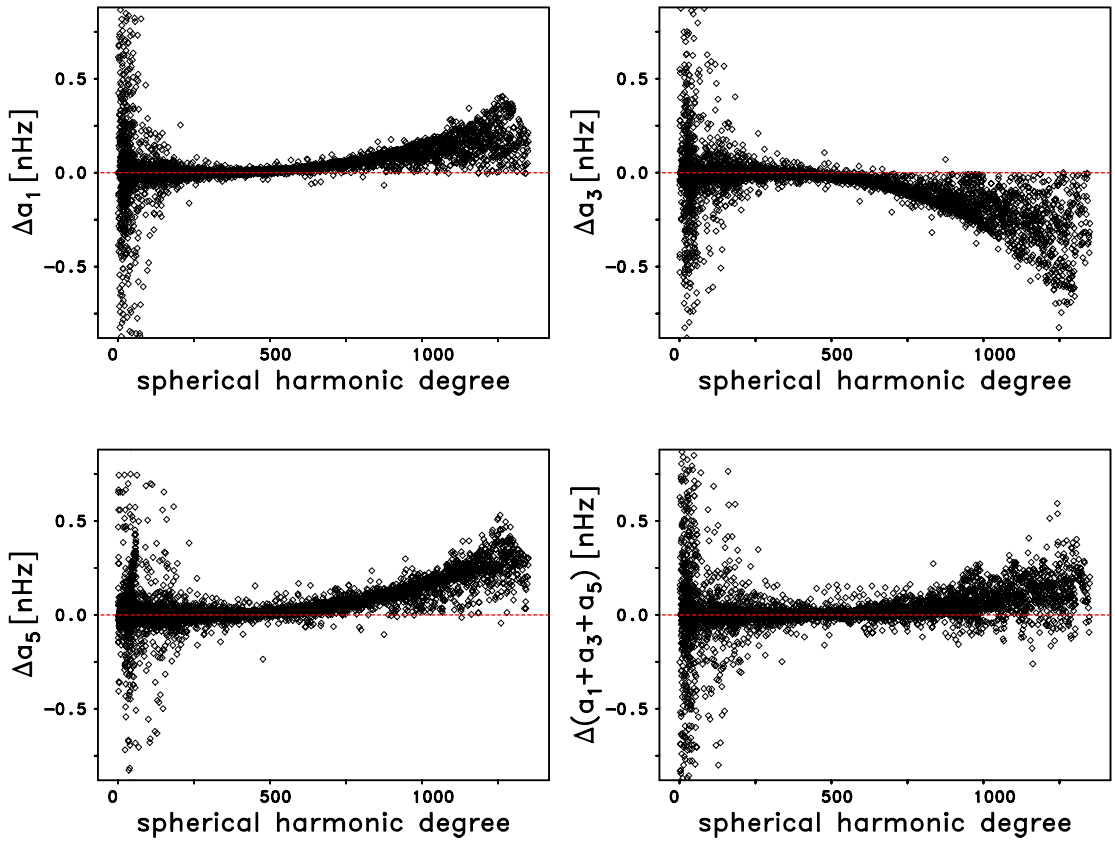

Figure 11: (Upper-left panel) Raw differences $\Delta a_1 = a_{1_{\mathrm{HMI.100430to0710.i.v0}}} - a_{1_{\mathrm{HMI.100430to0710.v7}}}$ of the frequency-splitting coefficients a_1 as functions of the spherical harmonic degree for the ridges $n = 0$ through $n = 30$. The dashed red line is for a difference of zero. (Upper-right panel) Same as upper-left panel, but for the frequency-splitting coefficients a_3. (Bottom-left panel) Same as upper-left panel, but for the frequency-splitting coefficients a_5. (Bottom-right panel) Same as bottom-left panel, but for the sum of the odd frequency-splitting coefficients $a_1 + a_3 + a5$.

The normalized splitting coefficient differences for the iplkm case are shown as functions of degree in Figure 12. All four panels in this figure look very similar to the corresponding panels in Figure 11. The two main differences in the two sets of differences are the fact that the iplkm coefficient differences are smaller than the corresponding Bang differences for degrees below about 750, while the iplkm differences are larger than the Bang differences at the higher degrees. These impressions can be confirmed by comparing the statistics in Table 4 with those in Table 3. The third column of Table 4 shows that the percentages of iplkm differences that exceeded $1\,\sigma$ were considerably smaller than the percentages of the Bang differences that also exceeded $1\,\sigma$. On the other hand, a comparison of the fourth columns of the two tables shows that the number of iplkm a_1 coefficients that exceeded $2\,\sigma$ was nearly 11 times larger than the corresponding number of Bang a_1 coefficients, and the comparison of the two fifth columns shows that the percentage of iplkm a_1 coefficient differences that exceeded $3\,\sigma$ was 23 time larger than the corresponding percent of Bang a_1 coefficients.

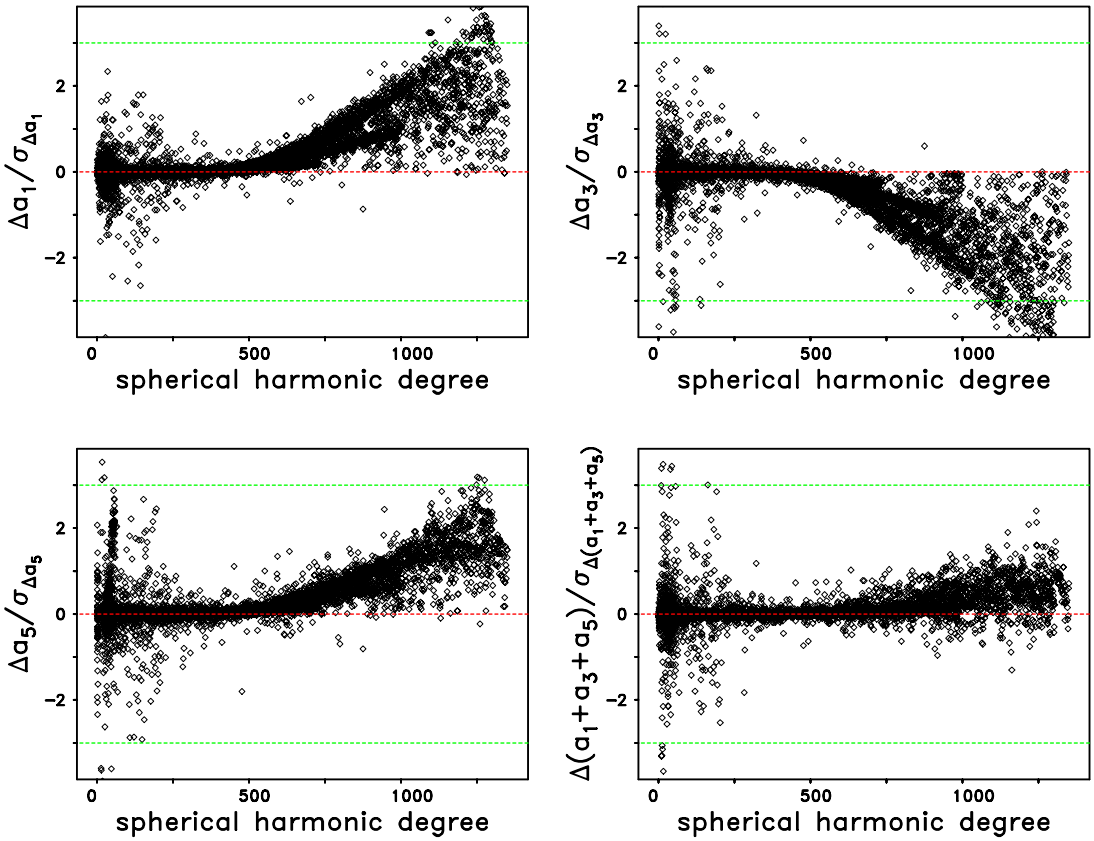

Figure 12: Same as Figure 11, but for the normalized differences $(a_{1_{\rm HMI.100430to0710.i.v0}} - a_{1_{\rm HMI.100430to0710.v7}})/\sigma_{\Delta a_1}$ The normalization was carried out by dividing the raw differences, Δa_1, as shown in the upper left-hand panel of Figure 11, by the formal error, $\sigma_{\Delta a_1}$, of each difference. The dashed green lines show the $\pm 3\,\sigma$ levels.

difference	#	$\% > 1\,\sigma$	$\% > 2\,\sigma$	$\% > 3\,\sigma$
a_1	7307	13.27	3.97	0.68
a_3	7283	15.72	5.99	1.94
a_5	7013	12.95	2.67	0.40
$a_1 + a_3 + a_5$	7013	2.97	0.61	0.23

Table 4: Statistics of the differences in the odd frequency-splitting coefficients as well as in their sum. In the 2nd column the number of commom cases is listed. The remaining columns give the percentages of cases for which the differences exceed the $1\,\sigma$, $2\,\sigma$, and $3\,\sigma$ level, respectively.

We show the binned raw coefficient differences as functions of degree in Figure 13. All four panels of this figure show that the differences in the iplkm coefficients were negligible for degrees below 500, while they increased systematically until reaching maximum values for degrees between 1200 and 1300. We show the binned normalized iplkm coefficient differences as functions of degree in Figure 14. The behavior of all four sets of normalized differences looks to be identical to the variation of the raw iplkm coefficients differences that were just shown in Figure 13. The overall maximum normalized iplkm coefficient difference is the one for the a_3 coefficient, which is nearly equal to $3\,\sigma$.

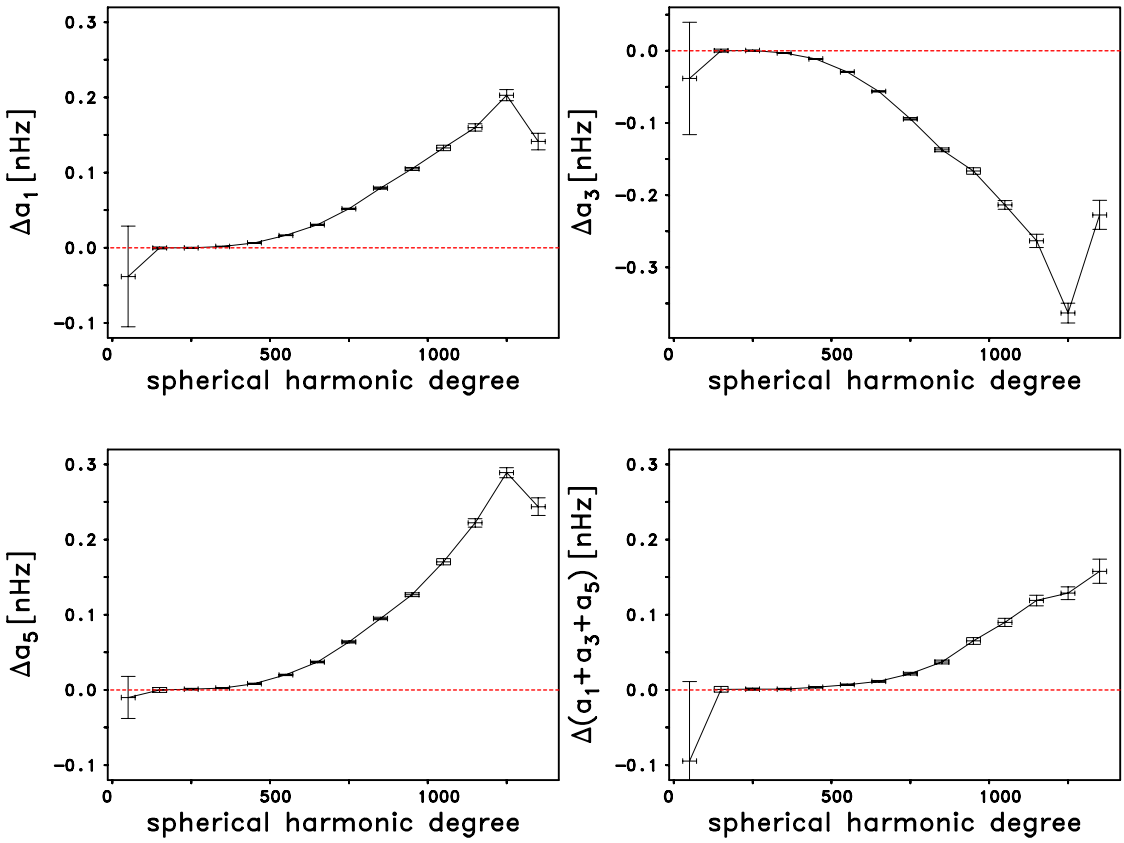

Figure 13: (Upper-left panel) Binned raw differences $\Delta a_1 = a_{1_{\mathrm{HMI.100430to0710.i.v0}}} - a_{1_{\mathrm{HMI.100430to0710.v7}}}$ of the frequency-splitting coefficients a_1 as functions of the spherical harmonic degree using 100-degree wide bins for the ridges $n = 0$ through $n = 30$. The dashed red line is for a difference of zero. (Upper-right panel) Same as upper-left panel, but for the frequency-splitting coefficients a_3. (Bottom-left panel) Same as upper-left panel, but for the frequency-splitting coefficients a_5. (Bottom-right panel) Same as bottom-left panel, but for the sum of the odd frequency-splitting coefficients $a_1 + a_3 + a5$.

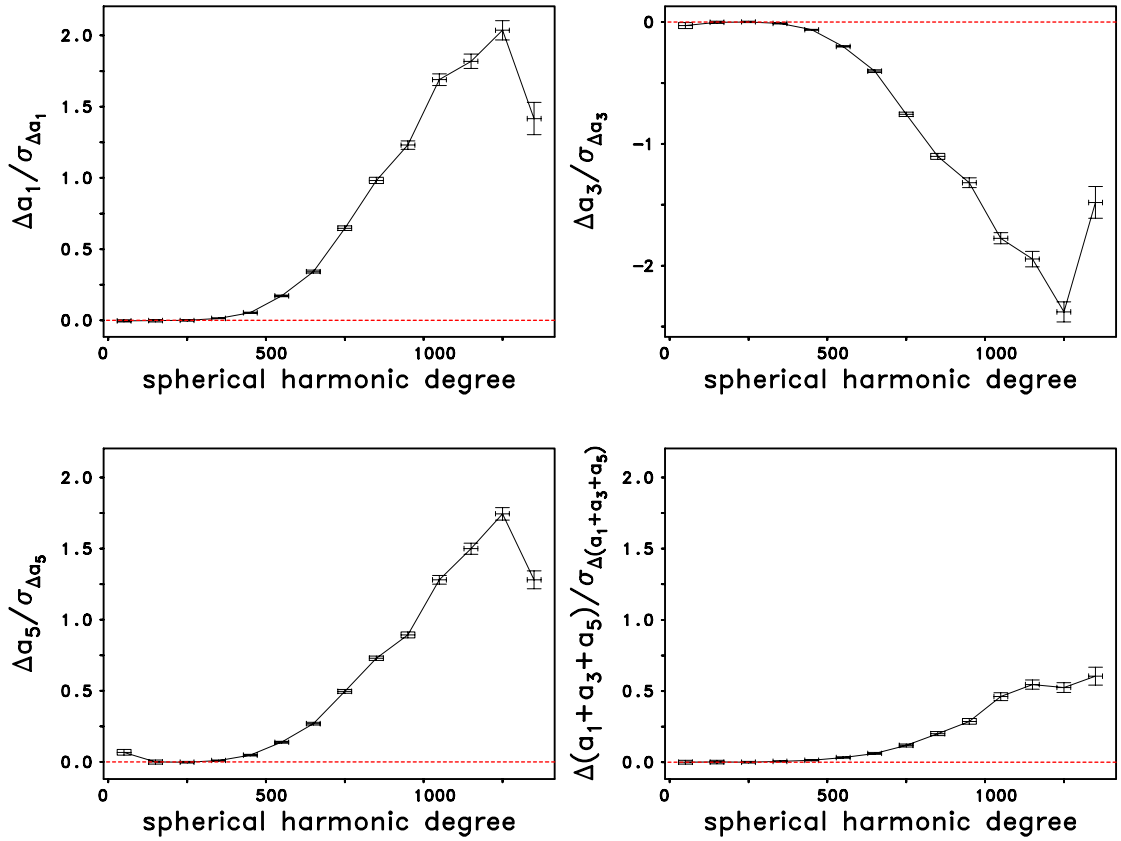

Figure 14: Same as Figure 13, but for the normalized differences $(a_{1_{\mathrm{HMI.100430to0710.i.v0}}} - a_{1_{\mathrm{HMI.100430to0710.v7}}})/\sigma_{\Delta a_1}$ The normalization was carried out by dividing the raw differences, Δa_1, as shown in the upper left-hand panel of Figure 13, by the formal error, $\sigma_{\Delta a_1}$, of each difference.

C) 72-Day averages of HMI B-angles for Future and Existing Tables of MPTS Frequency-splitting Coefficients.

The fact that the magenta and black sets of odd Bang frequency-splitting coefficients in Figure 1 have been demonstrated to be statistically different from each other suggests that leakage matrices need to be computed for additional values of the B-angle. Once we have been able to generate and employ additional leakage matrices in future MPTS fitting runs, we will be able to determine whether the differences in the splitting coefficients depend linearly upon the differences in the B-angle and we will also be able to determine whether the effects of these leakage matrices depend upon the sign of the B angle that is used to compute them.

In order to assist with the determination of the additional B-angles that should be employed in the generation of additional sets of leakage matrices, we have employed a file that Dr. Tim Larson kindly generated for us which gives the value of the FITS keyword CRLT_OBS at noon of each day of the HMI mission through March 16, 2023. This keyword gives the value of the Carrington Latitude, or B-angle, of the center of the solar disk as viewed by the HMI instrument. In Figure 15 we show the CRLT_OBS values as a function of MDI Day Number. In Figure 16 we show the absolute value of CRLT_OBS as a function of MDI Day Number. In Figure 17 we show the 72-day averages of CRLT_OBS for HMI Runs 1 through 65 (and the 24-day average of CRLT_OBS for Run 66) as a function of the MDI Day Number. In Figure 18 we show both the 72-day averages of CRLT_OBS and the 72-day averages of the absolute value of CRLT_OBS as a function of the MDI Day Number for the 16 HMI runs for which a table of MPTS splitting coefficients has already been generated.

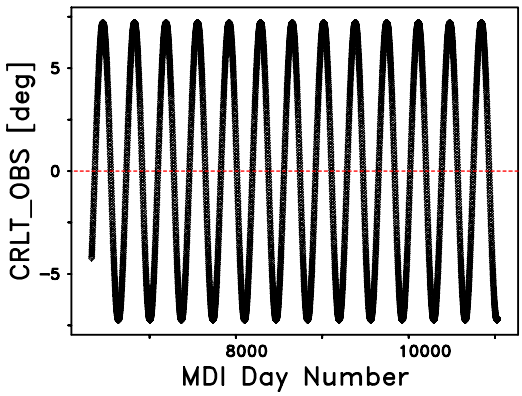

Figure 15: Value of CRLT_OBS as a function of the MDI Day Number. The dashed red line is for a value of CRLT_OBS = 0.

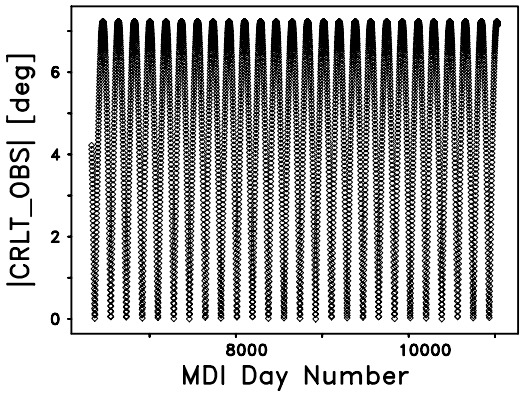

Figure 16: Absolute value of CRLT_OBS as a function of the MDI Day Number.

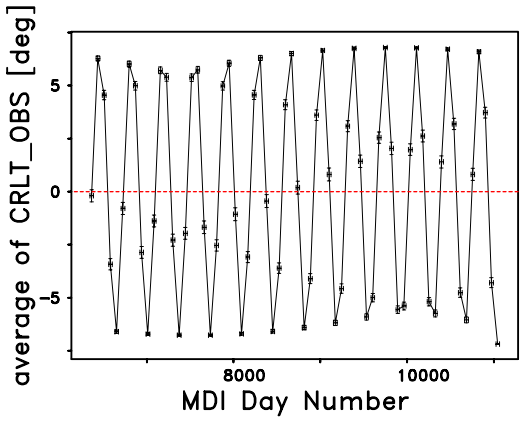

Figure 17: 72-day averages of CRLT_OBS for HMI Runs 1 through 65, and the 24-day average of CRLT_OBS for Run 66 as a function of the MDI Day Number. The error bars are the standard errors of the 72-day averages.

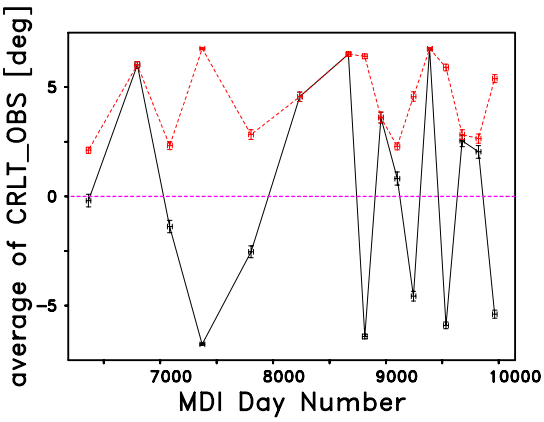

Figure 18: 72-day averages of CRLT_OBS (black) and 72-day averages of the absolute value of CRLT_OBS (red) as a function of the MDI Day Number for 16 HMI runs. The error bars are the standard errors of the 72-day averages.

Figure 18 shows that even if we determine that the absolute value of the B-angle is the relevant quantity rather than CRLT_OBS itself, five of these 16 runs for which the average of CRLT_OBS and the average of the absolute value of CRLT_OBS are identical, so some of these average values should be used to generate additional leakage matrices for testing. Figure 18 also shows that very few of these 16 runs corresponded to average values of B that were less than one degree. Rather, Table 5 shows that Dr. Larson's use of -6.354 degrees for the Bang test was definitely not too large in absolute value. In fact, regardless of whether the raw B values or the absolute values of B were averaged, four of the 16 cases had an average B value between 6.25 and 6.80 degrees in absolute value. Also, the first row of Table 5 shows that 12 of the 16 runs corresponded to average values of B that were greater than 2.5 degrees. The second row of Table 5 shows that when $|B|$ was averaged, 13 of the 16 runs corresponded to average values of $|B|$ that exceeded 2.5 degrees.

D) Conclusions

We believe that the statistics included Tables 1 and 2 and the information contained in Figures 1 through 7 indicate that the use of a non-zero B-angle in the generation of the leakage matrices that are employed in the MPTS method results in changes to the odd-order frequency-splitting

Qantity Averaged	# of Runs Between 0 and 2.5 degrees	# of Runs Between 2.5 and 5.0 degrees	# of Runs Between 5.0 and 6.8 degrees
B	4	6	6
$\|B\|$	3	6	7

Table 5: Distributions of the absolute magnitude of the average values of either B (row 1) or $|B|$ (row 2) for the 16 72-day HMI runs for which tables of fitted MPTS splitting coefficients and modal parameters now exist.

coefficients that will likely result in small, but systematic differences in the resulting rotational inversions. Furthermore, the average values of the B-angle and of the absolute values of B for the 16 HMI 72-day runs for which tables of fitted MPTS splitting coefficients already exist that are shown in Figure 18, and the statistics contained in Table 5, indicate that 75 % or more of those 16 HMI runs correspond to average B-angles that exceed 2.5 degrees in magnitude. These facts suggest that it will be important to compute additional leakage matrices for a range of additional non-zero values of the B-angle. That will correspond to other average values of the B-angle that were present during those 16 HMI 72-day time intervals. Once we have been able to generate and employ additional leakage matrices, we will be able to determine whether the differences in the splitting coefficients depend linearly upon the differences in the B-angle. We also think it will be important to employ another B-angle equal to +6.354 degrees so that we can investigate the effects that the positive B-angles will have on the splitting coefficients. We also believe that the statistics contained in Tables 3 and 4 and the panels contained in Figures 8 through 14 indicate that the use of interpolation in the generation of the leakage matrices will also result in small, but systematic differences in the splitting coefficients. Hence, we feel that we should not use interpolated leakage matrices in the future.